Gas-Phase Databases for Quantitative Infrared Spectroscopy

STEVEN W. SHARPE,* TIMOTHY J. JOHNSON, ROBERT L. SAMS, PAMELA M. CHU,* GEORGE C. RHODERICK, and PATRICIA A. JOHNSON

Pacific Northwest National Laboratory, P.O. Box 999, Richland, Washington 99352 (S.W.S., T.J.J., R.L.S.); and National Institute of Standards and Technology, Analytical Chemistry Division, 100 Bureau Drive, Stop 8393, Gaithersburg, Maryland 20899-8393 (P.M.C., G.C.R., P.A.J.)

The National Institute of Standards and Technology (NIST) and the Pacific Northwest National Laboratory (PNNL) are each creating quantitative databases containing the vapor-phase infrared spectra of pure chemicals. The digital databases have been created with both laboratory and remote-sensing applications in mind. A spectral resolution of ≈0.1 cm^{-1} was selected to avoid degrading sharp spectral features, while also realizing that atmospheric broadening typically limits line widths to 0.1 cm^{-1}. Calculated positional (wavenumber, cm^{-1}) uncertainty is ≤0.005 cm^{-1}, while the 1σ statistical uncertainty in absorbance values is <2% for most compounds. The latter was achieved by measuring multiple (typically ≥9) path length–concentration burdens and fitting a weighted Beer's law plot to each wavenumber channel. The two databases include different classes of compounds and were compared using 12 samples. Though these 12 samples span a range of polarities, absorption strengths, and vapor pressures, the data agree to within experimental uncertainties with only one exception.

Index Headings: **Database; Quantitative; Gas-phase; Infrared; Fourier transform infrared spectroscopy; FT-IR.**

INTRODUCTION

As Fourier transform infrared (FT-IR) spectroscopy has matured into a routine analytical technique,[1] the need has increased for reference data of high quality. In particular, national and international pressure for reduced anthropogenic emissions including hazardous air pollutants, greenhouse gases, and ozone-destroying chemicals has pushed quantitative infrared analysis to a new level of importance. For instance, the Environmental Protection Agency (EPA) has released Method TO-16 for the monitoring of atmospheric gases utilizing long, open-path Fourier transform infrared spectroscopy.[2] Also, EPA Method 320 describes the procedures required for extractive FT-IR measurements of vapor-phase organic and inorganic emissions.[3] In addition to FT-IR techniques, active open-path monitoring has also been performed using a variety of laser-based techniques.[4] For all such measurements, the need for accurate reference data is critical.

Some infrared spectral reference libraries already exist. In particular, databases that are compilations of individual molecular line transition parameters that allow positions, intensities, and line widths to be calculated as a function of concentration, pressure, temperature, path length, and resolution are available. The ATMOS,[5] GEISA,[6,7] and HITRAN[8] databases all contain information of this nature for molecules of atmospheric importance. For example, the HITRAN database has been in existence for more than 35 years and now contains over one million lines, i.e., rotational-vibrational transitions. As such, it provides an extremely useful resource for many researchers for a variety of applications ranging from simple comparative studies to sophisticated radiative transfer calculations.

For gas-analysis monitoring there also exist infrared libraries available from commercial and government sources, including Midac Corporation,[9] Infrared Analysis Corporation,[10] the U.S. Environmental Protection Agency,[11] Nicolet-Aldrich vapor-phase library,[12] and the National Institute of Standards and Technology (NIST).[13] With the exception of the NIST library,[13] we have found that the lack of sample quantification, chemical impurities, insufficient resolution or system noise, and nonlinearities have limited the usefulness of these spectra for either laboratory analytical work or quantitative remote sensing.

With these considerations in mind, PNNL and NIST[13] have independently undertaken projects to compile experimental databases specifically designed to quantify the mixing ratios of gas-phase species in either laboratory or remote-sensing applications. The most important features of the two data sets are summarized in Table I, with additional details provided in the Appendix. Finally, when establishing an absolute standard, an important consideration is to verify the result(s) by comparing the data to those obtained on other systems, preferably generated in a different fashion, so as to check for systematic errors. For a specific subset of molecules, NIST and PNNL have compared their respective data against one another.

EXPERIMENTAL

Instrumental and Data Acquisition. In describing both the experimental apparatus and the analysis methods, it must be mentioned that the FT-IR technique is fraught with errors and artifacts.[14] Some of the better-known effects include ghosting artifacts,[15] errors associated with the phase-correction method during the Fourier transformation,[16–18] source instability,[19] spectral aliasing due to an insufficient digitization rate, and the spectral artifacts that can arise from the detector's nonlinear response. The photoconductive mercury cadmium telluride (MCT) detectors used in the mid-infrared are particularly susceptible to nonlinear behavior, especially when operated at high light levels.[20–24] To minimize the MCT nonlinearity, we used a software correction supplied by the spectrometer manufacturer that maps the Fourier frequencies into their correct domains,[25] independent of the electronic bandwidth, thus compensating for the nonlinear behavior of the MCT. A further compensation for detector and other nonlinearities is designed into the data reduction, as described in the Data Analysis section.

Received 13 May 2004; accepted 27 July 2004.
* Author to whom correspondence should be sent. E-mail: sw.sharpe@pnl.gov, pmchu@nist.gov.

0003-7028/04/5812-1452$2.00/0
© 2004 Society for Applied Spectroscopy

TABLE I. Salient features of the NIST and PNNL gas-phase infrared databases.

Parameter	NIST	PNNL
Database emphasis	Greenhouse gases, EPA hazardous air pollutants, freons	Reactive compounds, industrial pollutants, DOE fossil and nuclear fuel remediation species
Spectral resolution	0.125 cm^{-1}	0.112 cm^{-1}
Minimal spectral coverage	3975 cm^{-1} to 575 cm^{-1}	6500 cm^{-1} to 600 cm^{-1}
Composite ordinate error (for standard compounds)	≤2.1%	≤2.1%
Noise level (at 10 μm)	≤0.005 ABS (base 10, RMS)	≤0.0005 ABS
Minimum number of path length–concentration burdens for 25 °C data	9	10
Sample preparation	Gravimetrically prepared, flow-through samples in White cell	Static pressure measurements using single pass sample cell
Web site	http://gases.nist.gov/spectral.html	http://nwir.pnl.gov

The spectrometers used for these measurements were Bruker IFS 66v/S models, both at NIST (one system) and at PNNL (two systems).† All are vacuum-bench spectrometers in order to minimize interference from spectral features due to H_2O and CO_2, as well as to provide more stable spectral baselines. As per the suggestion of the IUPAC committee on FT-IRs chaired by Bertie,[26] we have documented all relevant parameters associated with both data acquisition and data processing in a recent paper.[27] The more important operating criteria associated with the FT spectrometers and data acquisition are compiled in Table II. We note that we have modified the PNNL spectrometer systems to correct for two artifacts that introduce photometric errors, both of which find their origin at the aperture.[27] The first error arises from light that has already been modulated by the interferometer returning toward the source and then being reflected by the back of the metal aperture wheel into the interferometer to be modulated again. This double modulation produces an optical $2f$ alias that can add spurious signals and distort intensities at all wavelengths. A second artifact was originally noted by Johns[28] and Giver et al.;[29] they pointed out that at high resolution a cooled (MCT) detector sees not only the source, but also the aperture annulus that is near room temperature, and this metal annulus effectively serves as a blackbody radiator. These blackbody rays do not satisfy the resolution condition since they enter the interferometer as off-axis rays; the effect in spectral space is a distorted absorption line shape that shows a ''tailing'' to lower frequencies. The PNNL spectrometers have both been modified to remove these two effects by adding a second aperture (optical stop) after the interferometer; the NIST system is not as susceptible to these artifacts due primarily to the use of a White cell. It is thought that the transfer optics of the NIST White cell acts as an optical stop, similar to the second aperture on the PNNL system. The magnitudes of the ''$2f$ modulation'' and ''warm aperture'' intensity errors for moderate resolution (0.1 cm^{-1}) features were approximately 3% and 12%, respectively. Clearly the magnitude of the corrections will depend on the desired resolution, as well as on the optical configuration in each instrument.

Positional (Wavenumber, cm^{-1}) Calibration. A strict requirement of both databases is to accurately calibrate the reference data on the x-axis. All data are of course referenced to the interferometer laser, but in order to achieve absolute accuracy both PNNL and NIST calibrate the spectrometer's measured frequencies against secondary frequency standards. The techniques are similar: NIST uses 158 specific water lines (the ν_3 asymmetric

† Certain commercial equipment, instruments, or materials are identified in this paper to foster understanding. Such identification does not imply recommendation or endorsement by the National Institute of Standards and Technology, nor does it imply that the materials or equipment identified are the best available for the purpose.

TABLE II. Experimental parameters for gas-phase measurements.

Parameter	NIST	PNNL
Spectrometer	Vacuum: Bruker IFS 66v	Vacuum: Bruker IFS 66v/s (two units)
Source	SiC glow bar	SiC glow bar
Beamsplitter	KBr	KBr extended range
Detector	Photoconductive mercury cadmium telluride (MCT)	Photoconductive mercury cadmium telluride (MCT)
Apodized resolution	0.125 cm^{-1} (0.9/optical path difference)	0.112 cm^{-1} (0.9/optical path difference)
Jacquinot stop aperture setting	2.0 mm	1.5 mm
Sample cell	7.5 L variable path White cell (used with three burdens each at 1.356, 3.998, and 9.282 ± 0.01 m). KBr windows	19.94 cm or 19.96 cm gold-plated thermostatted cell, used for ≥10 different burdens. Windows: wedged KBr, KCl or ZnSe
Sample form	Gravimetrically prepared, diluted in N_2, continuously flowing, typically 50 μmol/mol in N_2 at 1 L/min	Single static pressure measurement in cell, backfilled with N_2, sample typically 0.1 to 13 kPa of sample
Sample ballast gas	UHP N_2	UHP N_2 to (101.2 ± 0.7) kPa (760 ± 5) torr
Sample temperatures	23 °C; 25 °C to 200 °C for select species (all ±0.1 °C)	5 °C; 25 °C; 50 °C (all ±1 °C)
FT phase correction, zerofill	Mertz, 2× zerofilling	Mertz, 2× zerofilling
FT apodization function	Boxcar	Boxcar

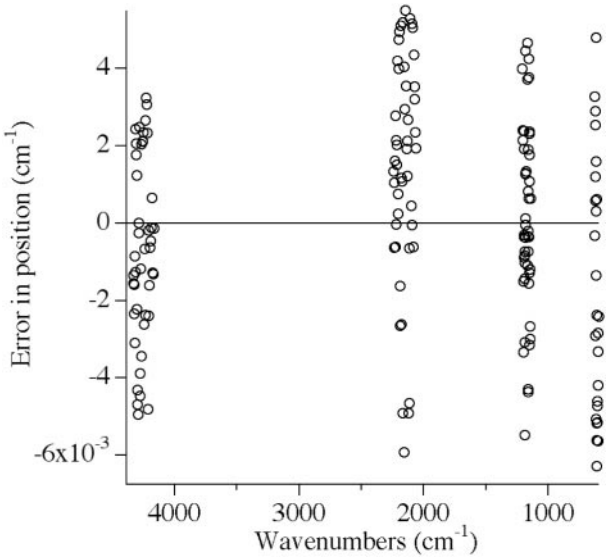

FIG. 1. Positional (wavenumber, cm^{-1}) errors versus position of individual reference transitions (CO and N_2O) after applying linear calibration correction. See text for details.

stretch near 3600 cm^{-1} and ν_2 symmetric bend near 1600 cm^{-1}) as measured by Toth to generate a linear correction.[30] PNNL uses 165 specific lines using carbon monoxide fundamental and overtone lines (2143 cm^{-1} and 4250 cm^{-1}) as well as nitrous oxide lines (in the 1170 cm^{-1} and 610 cm^{-1} region) as reported by Maki and Wells to generate a wavelength correction.[31] The positions of the selected transitions are derived from a fit of the individual absorbance profile. These spectra are measured at low pressure (typically 133 Pa to 2.66 kPa or 1 torr to 20 torr), and the positions of the reference spectra are generally accurate to 5×10^{-5} cm^{-1}. The position correction consists of applying a linear correction to the observed transitions that best correct the observed lines to the accepted value. The root-mean-square (RMS) deviation between corrected and reference line positions for NIST and PNNL are 0.0042 cm^{-1} and 0.0018 cm^{-1}, respectively. A plot of the PNNL corrected line positions minus the line positions versus the line position as reported by Maki[31] may be seen in Fig. 1. The wavelength calibration procedure is repeated after any alignment or adjustment to the spectrometer optics.

Sample Preparation and Delivery. Richardson and Griffiths also suggested the need for quantitative data in both laboratory and open-path IR measurements and have discussed the relative merits of different sample preparation methods that could be used to create a quantitative database such as the two described here.[32] The PNNL and NIST laboratories intentionally use different techniques to generate an accurately quantified number of molecules (absorbers) in the infrared beam: briefly, NIST uses gravimetric standards prepared in conjunction with the NIST Standard Reference Materials program in large gas cylinders and delivers the gas to the sample cell in a continuously flowing mode,[13] whereas the PNNL system is based on a single pass, static sample cell with sample number densities based on measured pressure values. Both systems have been designed to minimize the many errors associated with sample preparation, namely (1) non-quantitative sample transfer or incomplete gas mixing, (2) sample gas impurities, and finally (3) ''sticking'', i.e., sample or ballast gases (differentially) adhering to system components.[33]

The NIST gravimetric-flowing system uses a White cell that is typically used at three path length settings: 1.36 m, 4.00 m, and 9.28 m ($\pm$0.01 m). For each of these path lengths three different gas concentrations are flowed through the system for a total of nine path length $\times$ concentration products. Liquid samples are prepared as follows. An evacuated, aluminum gas cylinder is weighed to an accuracy of 0.1 g on a top-loading balance with a capacity of 32 kg. The cylinder is fitted with a CGA-350 adaptor that contains a septum and allows injection of the sample directly into the cylinder. Pure sample is drawn into a gas-tight syringe and weighed on a microbalance (100 g capacity) to an uncertainty of 5 μg. In order to assure complete vaporization of the sample, the septum and valve are heated to 80 °C during sample injection into the evacuated cylinder. After injection, the empty syringe is then re-weighed to determine the net sample weight. Once the sample has been introduced, the cylinder valve is closed and the septum removed. A specified pressure of ultra-high-purity (UHP) nitrogen is added to the cylinder; the cylinder is then re-weighed. The total mixing ratio of sample to nitrogen is determined as a micromole fraction, μmol/mol. Typically, samples range from 1 μmol/mol to 1000 μmol/mol depending on the IR band strengths and the sample vapor pressure. For samples ranging from 50 μmol/mol to 1000 μmol/mol, the expanded uncertainty is 0.2%. Samples up to 50 μmol/mol have an expanded uncertainty of 0.5%.

At NIST, compounds that are gaseous at room temperature require a different preparation procedure. A 150 mL stainless steel cylinder and the cylinder containing the pure gas analyte are connected to a gas manifold. The manifold and all the transfer lines to the cylinders are evacuated. Purging of the system with the pure gas compound is performed several times. An aliquot of pure gas analyte is transferred to the 150 mL stainless steel cylinder and then weighed a minimum of three times. The aluminum cylinder used for the standard preparation is evacuated and weighed. Both cylinders are connected to the gas manifold and the system evacuated. The analyte is transferred from the 150 cc stainless cylinder to the large aluminum cylinder. After closing the stainless steel cylinder valve, the residual in the transfer lines is purged into the aluminum cylinder with pure nitrogen balance gas. The stainless steel cylinder is removed and weighed a minimum of three times, with the resulting difference being the amount of analyte added to the aluminum cylinder. Nitrogen balance gas is then added to the aluminum cylinder to a predetermined pressure and weighed a final time. The concentration of the compound of interest is calculated from the molar data of the analyte and nitrogen. Using ethylene at 500 μmol/mol as an example, $\approx$2 g of ethylene would be needed to make this concentration in a 30 L cylinder with a final pressure of 12.4 MPa (1800 psi). The uncertainty in weighing this amount of material and the nitrogen, plus the uncertainty in the purity of the analyte and balance nitrogen, would be $\pm$0.1% (95% confidence interval, $k = 2$). For an ethylene standard at 50 μmol/mol, the resulting uncertainty would

be ±0.2%. For either gaseous or liquid samples, once prepared the standard is allowed to convectively mix inside the cylinder by placing a heat source at the base of the cylinder.

The PNNL infrared absorption cell is a single-pass design with wedged windows (KBr, ZnSe, or KCl). The sample cell length is measured at three points to ±0.1 cm with a nominal length of 20 cm. The sample cell and gas manifold are electro-polished and gold plated to reduce sample adhesion and possible decomposition. The cell is constructed with a 5.1 cm inside diameter and with a concentric 7.6 cm outside diameter temperature-regulated water jacket; a four-lead resistance platinum transducer with an accuracy of ±1 °C is used to monitor temperature. In order to minimize dead volume and the resulting errors during nitrogen backfill, the cell shut-off valve is located within 1 cm of the cell body. The ''dead volume'' for this 0.64 cm diameter × 1 cm long tube is approximately 0.1% of the total cell volume.

The PNNL samples are prepared and the pressures of the neat analyte are measured in the sample cell, so as to calculate the number-density of absorbers in the sample cell directly. This avoids the potentially serious problems associated with serial dilution(s) followed by transfer(s). The sample is back filled (diluted) with nitrogen from an all-metal stainless steel manifold that has been electropolished and gold plated to minimize sample adsorption or reaction with the surface; the manifold is maintained at ≈60 °C to facilitate sample outgassing. Three Baratron-type capacitance monometers (NIST traceable) with a full-scale accuracy of 0.05% are connected to the manifold via stainless steel lines. The three Baratrons have full-scale pressure readings of 0.133 kPa, 1.33 kPa, and 133 kPa (1 torr, 10 torr, and 1000 torr). The manifold is in turn connected to the sample cell mounted directly in the spectrometer sample compartment. The manifold and sample cell can be evacuated to 10^{-3} Pa (10^{-5} torr) via a liquid nitrogen trapped diffusion pump. Both the sample cell and pumping system can be independently isolated from the manifold via gate-valves. UHP nitrogen is supplied to the manifold through a computer-operated leak valve, with water previously removed from the nitrogen by flowing the gas through a small-bore copper tube immersed in liquid nitrogen.

A sample is prepared by placing approximately 10 g to 20 g of neat sample into either a 50 mL stainless steel or glass finger mounted to the manifold. For gaseous samples, several atmospheres of neat sample are placed into the manifold, and then condensed into the finger cooled to 77 K. All samples undergo several freeze–pump–thaw cycles to remove air. In addition, and depending on sample purity, the sample is cooled with a slush bath such that the vapor pressure of the sample is slightly less than 0.1 kPa (1 torr) and then pumped on for several minutes to remove any of the more volatile contaminants. If additional purification is required, the sample is then distilled to a second cold finger. In some cases, the sample will have trace water dissolved in it; if so, a desiccant such as $CaSO_4$ is used. The desiccant–sample is typically allowed to sit overnight, thus thoroughly drying the sample and allowing any CO_2 gas in the desiccant to outgas. If a sustained outgassing is observed, CO_2 is also pumped away before introducing each aliquot of vapor-phase analyte to the sample cell.

Once the sample is purified of air and other impurities, the pumping system is isolated and the sample is admitted to the manifold/absorption cell. Depending on the infrared band strength and vapor pressure of the sample, the manifold and cell are filled to a specified target pressure with sample. The finger is valved off from the manifold and the pressure allowed to stabilize such that the pressure change is less than 0.5% in 1 min. At this point, a final pressure reading is taken, the cell temperature noted, and the sample cell is closed and isolated from the manifold. The manifold is pumped out, purged with UHP nitrogen, and re-evacuated. The sample cell must then be backfilled to 101.3 kPa (1 atm) with UHP nitrogen while avoiding sample backflow from cell to manifold; the backfill process begins by pressurizing the manifold to ≈30 kPa (200 torr) with UHP nitrogen and only then opening the manifold/cell valve. The nitrogen flow is continued until the manifold and cell reach a pressure of approximately 96 kPa (720 torr) at which point the valve is closed, isolating the cell from the manifold. The manifold is further pressurized to approximately 103 kPa (770 torr) and the nitrogen flow turned off. The cell is opened to the manifold for a very brief burst, allowing the last N_2 to flow in, such that the final cell pressure is 101.3 kPa (760 torr) ±0.7%. The validity of the procedure has been established by trial and error. To monitor for condensation of the analyte during the nitrogen pressurizing process (i.e., for burdens near the dew point), the IR absorption signal is monitored before and after nitrogen gas addition to make sure any analyte condensed during the nitrogen backfill is re-vaporized. To avoid much of the tedium and to minimize operator mistakes, the entire process of backfilling, system purge, and pump-out is performed via a computer interfaced to the gas manifold. The process is repeated for multiple concentrations of analyte per sample, typically twelve at 25 °C and six each at 5 °C and 50 °C.

DATA ANALYSIS

All data are corrected on the positional axis using the linear correction factors generated from the reference gases as described above. For the intensity values, the data are reduced by constructing a Beer's law plot at each positional bin (wavenumber, cm^{-1}) and determining the slope using a classical, linear, least-squares approach.[34] At each positional bin, the absorbance $A_i(\nu)$ is plotted versus the mixing ratio C_i for the i measured burdens:

$$A_i(\nu) = \varepsilon(\nu) dC_i \tag{1}$$

The result is a linear plot yielding the absorption coefficient $\varepsilon(\nu)$ from the fitted slope. However, in order to minimize the known nonlinearities associated with FT-IR absorption measurements, a data weighting scheme is used in which each measured absorption value is weighted according to $T_i^2(\nu)$ ($A = -\log T$), and all data with $A(\nu) \geq 1.6$ ($T \leq 0.025$) are assigned a weight of zero.[13] The effect of the weighting scheme is that for strong absorption features, linear behavior is obtained by favoring the low-burden measurements, whereas for weaker bands good signal/noise is derived from the high-burden mea-

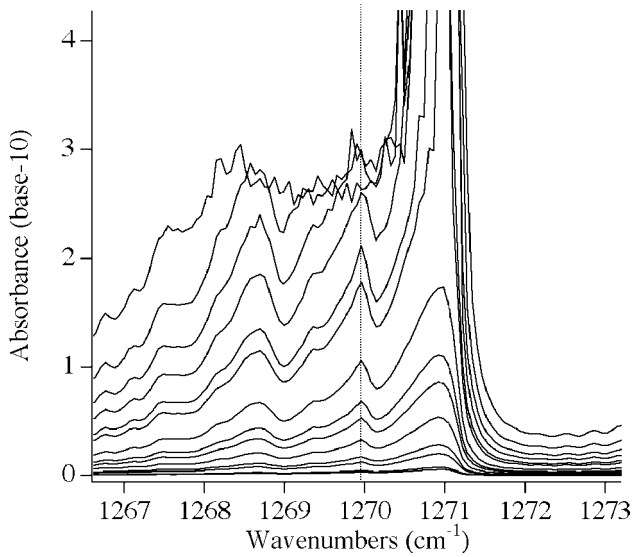

FIG. 2. Small spectral region corresponding to sulfuryl fluoride, taken at different partial pressures of sulfuryl fluoride. The vertical dashed line represents the position of a single positional channel used in the following example of the Beer's law fit described in the text.

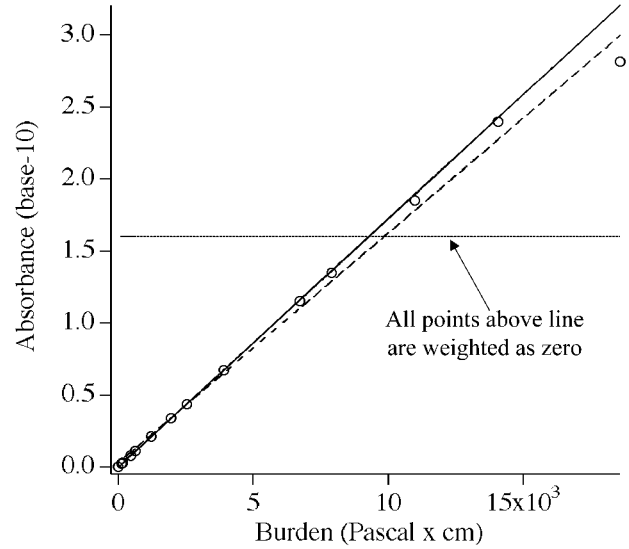

FIG. 3. Curve of growth for the absorbance of sulfuryl fluoride at the position (wavenumber, cm^{-1}) specified in Fig. 2. The solid line represents the weighted linear least squares fit while the dashed line is the corresponding un-weighted fit.

surements (in which the strong peaks are either down-weighted or discarded altogether). Figure 2 illustrates the procedure using sulfuryl flouride, SO_2F_2; this figure contains 14 plots with partial pressures of SO_2F_2 ranging from 8.27 Pa to 13 985.54 Pa (0.062 torr to 104.9 torr). The dashed vertical line in Fig. 2 indicates the selected wavenumber bin at $\approx$1270 cm^{-1} used for the example of the Beer's law plot appearing in Fig. 3. It is seen that for the strong features to the higher frequency, linear behavior is obtained by favoring the smaller burdens where the absorbance values are $\leq$1.6. But for the weaker features to lower frequency, the best signal-to-noise ratio is obtained from the high concentration measurements. A corresponding curve-of-growth for absorbance versus concentration of absorber, at the selected positional bin ($\approx$1270 cm^{-1}) may be seen in Fig. 3. The solid line represents the best linear fit through the points using the weighting scheme discussed above. An unweighted linear fit is represented by the dashed line. Note the deviation of the two lines at higher absorbance (concentration) value is indicative of nonlinear effects. The method thus takes advantage of the full dynamic range of the instrument and obtains a far more linear spectrum than can be derived from any single measurement. In addition to better linearity, using multiple burdens greatly increases the signal/noise ratio (SNR). For strong features, the SNR can exceed 10^6.

In addition to the fitted (composite) spectral vector, a deviation vector is generated during the weighted, linear least squares fitting process. This deviation vector is simply the statistical uncertainty in the weighted linear least squares fit. An example of the deviation vector plotted against the fitted absorbance values for SO_2F_2 appears in Fig. 4. Note that the larger deviations occur at the higher absorbance values. Any spectral features that do not scale linearly with sample concentration will exhibit a poor fit and consequently larger deviation values. The deviation vector thus provides an inherent and sensitive probe for chemical impurities. During the course of a measurement series, the temperature of the sample reservoir will change. Since it is unlikely that potential impurities in the sample will have identical volatilities to those of the sample at several temperatures (Henry's Law), the relative amount of impurity vapor will not scale the same as the sample vapor pressure. Moreover, the mole fraction of any higher volatility impurity tends to decrease with time. A chemical impurity signature is thus easily recognized in the deviation vector. An example of ethene impurity in the fitted spectrum of SO_2F_2 appears in Fig. 5. Referring to this figure, the deviation vector (middle trace) for SO_2F_2 contains several features corresponding to ethene that are not obvious in the fitted spectrum of SO_2F_2. A reference spectrum of ethene is included (upper

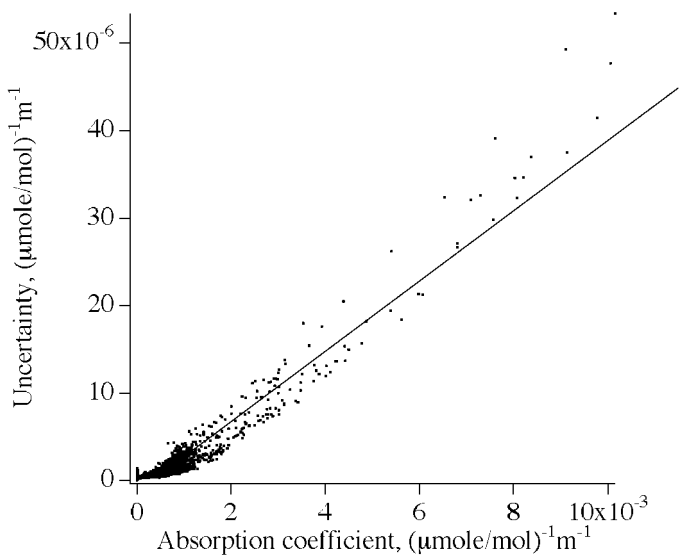

FIG. 4. Plot of uncertainty in fitted absorption coefficient versus fitted absorption coefficient. Note that each point corresponds to a unique positional (wavenumber, cm^{-1}) value. The slope of this line is an average statistical uncertainty in the absorption coefficient.

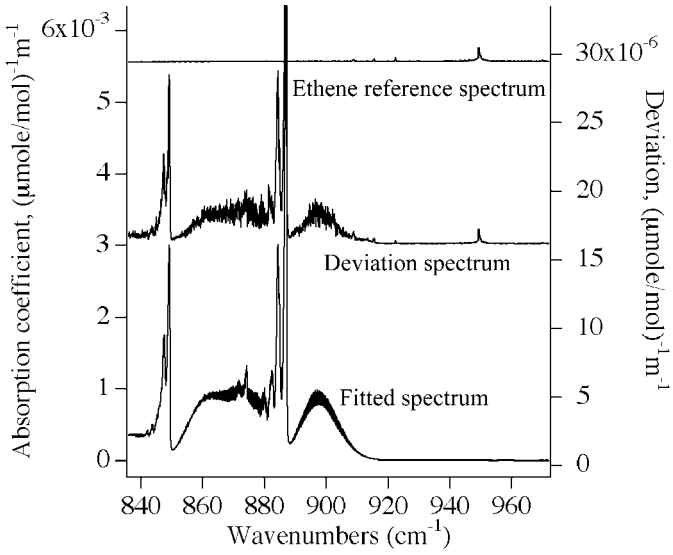

FIG. 5. Example of using the deviation vector to identify impurities in the sample. Lower trace: fitted spectrum of SO_2F_2; middle trace: deviation or uncertainty vector; upper trace: reference spectrum of ethene. Ethene contamination is approximately 0.01% (P/P) of total sample.

trace) for comparison purposes in Fig. 5. Note that the deviation vector is plotted as per the right-hand axis.

For statistical (type *A*) errors, the deviation vector describes random uncertainties associated with the measurements. In order to estimate the magnitude of the systematic (type *B*) uncertainties, the maximum uncertainty of individual experimental parameters must be estimated. Fractional value estimates of the uncertainties associated with the experimental parameters are compiled in Table III. So long as these experimental factors are uncorrelated, the fitted composite uncertainty associated with the instrumental parameters can be calculated as follows:

$$\mu_{\mathrm{Bias}} = k[(\mu_{\mathrm{L}})^2 + (\mu_{\mathrm{T}})^2 + (\mu_{\mathrm{P}})^2 + (\mu_{\mathrm{BL}})^2 + (\mu_{\mathrm{N}})^2]^{1/2} \quad (2)$$

where $k = 2$ is chosen at the 95% confidence limit (2σ). For the present analysis, we estimate $\mu_{\mathrm{Bias}} = 2.3\%$. Assuming that the systematic uncertainties between the two laboratories are of the same magnitude and uncorrelated from each other, then

$$[(\mu_{\mathrm{Bias}_{\mathrm{NIST}}})^2 + (\mu_{\mathrm{Bias}_{\mathrm{PNNL}}})^2]^{1/2} = 3.2\% \quad (3)$$

The 3.2% value provides a gauge as to whether measurements between the two laboratories are within the expected 2σ deviation. It is emphasized again that two entirely different methods of sample generation and quantitation were employed, yet the data should agree to within these uncertainty estimates.

STABILITY AND LINEARITY OF INTENSITY MEASUREMENTS

In addition to the random (type *A*) and systematic (type *B*) uncertainties discussed above, additional analysis was undertaken to experimentally characterize both the stability and the linearity of the measurements. The stability measurement quantifies the degree of instrumental drift and *in situ* chemical adsorption/desorption, and for that reason the study was conducted using a polar molecule, namely methanol. Figure 6 presents the percent change

TABLE III. Potential sources of systematic uncertainties in spectral measurements.

Parameter	Symbol	Estimated fractional value
Optical path length	μ_{L}	0.005
Sample temperature	μ_{T}	0.002
Sample pressure	μ_{P}	0.001
FT-IR baseline drift	μ_{BL}	0.002
MCT nonlinearity	μ_{N}	0.01

(from zero-time) in the integrated absorption values for a series of measurements made on the same methanol (163.72 Pa, 1.228 torr) plus nitrogen sample in the PNNL 20 cm cell at 298.2 K. The region selected for integration corresponds to the C–H stretch of methanol, between 2700 cm^{-1} and 3200 cm^{-1}. Each measurement (data point) required ≈4 min to acquire. The total duration of the series was ≈30 min, significantly longer than the time required (≈9 min) to measure a typical spectrum. As can be seen in Fig. 6, the variation in integrated intensity is ±1% or less for all points. Much of the scatter is attributed to baseline stability with a slight trend seen for decreasing integrated area. This downward trend is perhaps due to adsorption of the methanol onto the cell walls and windows.

In order to cover the lower frequency spectral region (1200 cm^{-1} to 600 cm^{-1}) at higher resolution, it is necessary to use a cooled, photoconductive MCT detector. Unfortunately, MCT detectors are known for their nonlinear response.[20,23] To investigate the degree to which the Bruker software correction in combination with the data weighting scheme mitigated the effect of detector nonlinearity, additional experiments were conducted using detectors known to have linear responses to photon fluence. Both a liquid nitrogen cooled, indium antimonide (InSb) detector and a room-temperature deuterated try-glycine sulfate (DTGS) detector were utilized for these compar-

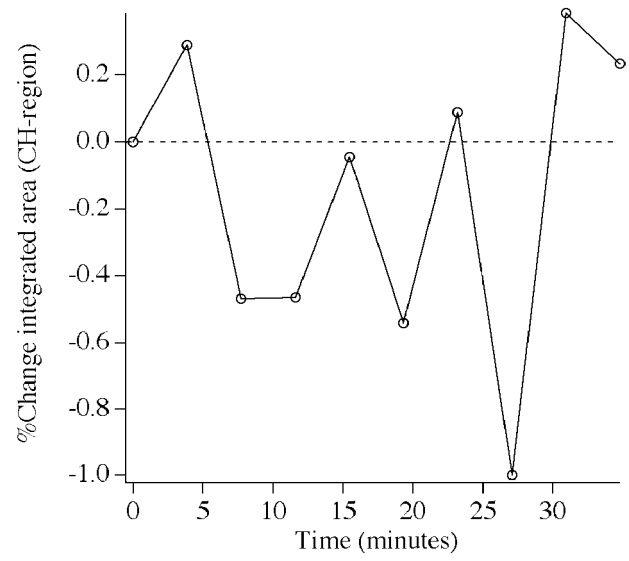

FIG. 6. Results corresponding to the stability test of a polar sample (methanol) sitting in the sample cell. The percent change in integrated band area for the C–H stretch region of methanol is plotted against time, where integrated area at zero time is chosen for the reference value.

TABLE IV. Comparison of integrated band strength measurements (ethene and isopropanol) for MCT detector with nonlinearity correction with InSb and DTGS detectors. Values correspond to percent change from MCT measurements. %Change = (Area$_X$ − Area$_{MCT}$)/Area$_{MCT}$ × 100. Data are presented in the mid-wavelength infrared (MWIR) and long-wavelength infrared (LWIR) regions.

Detector	MWIR band area, C_2H_4 (3300–2900) cm^{-1}	LWIR band area, C_2H_4 (1150–800) cm^{-1}	MWIR band area, IPA (3100–2800) cm^{-1}	LWIR band area, IPA (1600–760) cm^{-1}
InSb	+1.97%	NA	−0.04%	NA
DTGS, $\Delta\nu$ = 1.0 cm^{-1}	+2.32%	+0.11	−0.38%	−2.21%

ison studies. Since the photovoltaic InSb has no response below ≈1850 cm^{-1}, it was only possible to compare intensities in the C–H stretching region. In addition, the D* values of the DTGS pyroelectric detector are two orders of magnitude poorer than a comparable MCT or InSb detector, but the useful spectral range (400 cm^{-1} to 6000 cm^{-1}) is nearly identical to MCT detectors. Despite the poorer sensitivity of the DTGS detectors, they are known to have a linear response over many orders of magnitude. For these DTGS measurements, instrument resolution (interferometer travel) was decreased to 1 cm^{-1}, while all other parameters were left unchanged. The 1.0 cm^{-1} resolution thus allowed the data to be acquired in a reasonable time and still yield decent signal-to-noise ratios. Ethene and 2-propanol (IPA) were chosen as the samples for detector comparison since they are both relatively inert and easy to handle. Samples of ethene and IPA were prepared and the data were analyzed as described earlier. All spectroscopic collection and FT parameters were left as shown in Table II, save that for the InSb and DTGS measurements the software nonlinearity correction was not employed.[25]

The results of the linearity investigations are summarized in Table IV. As can be seen from the table, the integrated band strengths are all in excellent agreement, under the 3% composite uncertainty value. Thus, the combination of the FT correction algorithm (for the MCT detector) combined with the multiple burden measurement followed by a $T(\nu)^2$ weighting scheme yields absorption cross-sections that scale linearly with optical depth. The results have been found to follow the Beer–Lambert law over many orders of magnitude. Although the comparison measurements were made with the nonreactive compounds ethene and isopropanol (IPA), the experiments were undertaken only to assess whether there was a linear response from the instrument (detector). The detector correction algorithm in combination with the weighting scheme clearly has an acceptably linear response at all wavelengths.

RESULTS AND DISCUSSION

Perhaps the most meaningful test of absolute accuracy is through independent, cross-laboratory comparison. A total of 12 different chemicals and 26 corresponding bands were selected to compare the results of NIST to those of PNNL and results are summarized in Table V. The samples were selected so as to contain both polar (e.g., methanol, ethylene oxide) and non-polar compounds (e.g., butane, benzene), strong (CCl_4) and weak absorbers (butane and SO_2), as well as both high (ethene) and low (n-butanol) vapor pressure species.

The last column in Table V contains the percent change (%Δ) for the integrated band areas of the PNNL versus

TABLE V. Integrated band strengths of selected molecules for intercomparison. %Δ = (PNNL − NIST)/NIST × 100.

Name (sample #)	Region (cm^{-1})	Area PNNL	Area NIST	%Δ
2-Propanol (1)	743–1571	0.043581	0.0432745	+0.71
	2511–3085	0.032155	0.0324211	−0.82
Benzene (2)	620–725	0.018597	0.0188219	−1.20
	2980–3150	0.01321	0.0133472	−1.03
Butane (3)	1198–1781	0.005769	0.0057734	−0.07
	2763–3065	0.055606	0.0563196	−1.27
n-Butanol (4)	656–1600	0.037514	0.0370135	+1.35
	2507–3266	0.054813	0.0545087	+0.56
	3558–3933	0.004176	0.0042139	−0.89
Carbon tetrachloride (5)	700–850	0.068585	0.0723102	−5.15
Freon-12 (6)	625–800	0.023179	0.0240156	−3.48
	1220–1310	0.005571	0.0056223	−0.91
Ethene (7)	797–1167	0.015677	0.0159012	−1.41
	2887–3295	0.007393	0.0074687	−1.02
Ethylene oxide (8)	2820–3378	0.0158493	0.0157895	+0.38
	1207–1340	0.0024165	0.00238196	+1.45
	720–985	0.0134701	0.0131431	+2.49
Methanol (9)	892–1762	0.026104	0.0261716	−0.26
	2513–3150	0.023001	0.023435	−1.85
Sulfur dioxide (10)	1037–1267	0.004101	0.0041552	−1.31
	1275–1420	0.031823	0.0320814	−0.81
	2411–2545	0.000648	0.0006574	−1.46
Toluene (11)	636–820	0.012361	0.0124424	−0.65
	2690	0.023177	0.0232127	−0.15
Trichloroethene (12)	729–1050	0.034118	0.0345095	−1.13
	3036–3213	0.00172543	0.00169687	+1.68

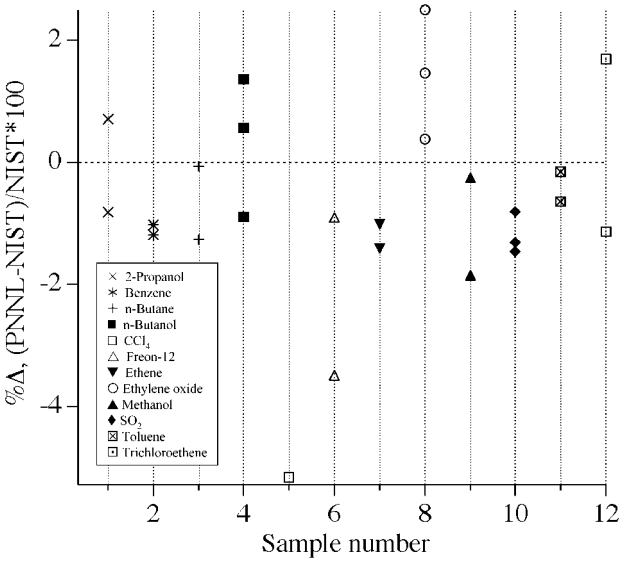

FIG. 7. Comparison between NIST and PNNL of the integrated band areas for 12 different samples. Sample number is defined in Table V.

NIST data. A plot of %Δ versus sample number can be seen in Fig. 7. It reveals that the PNNL integrated band areas are, on average, slightly smaller than the corresponding NIST values, with an average %Δ = −0.63% and an rms = 1.66. In an effort to identify possible causes for the discrepancies, %Δ was plotted against a number of sample parameters including molecular mass, gas-phase dipole moment, integrated band area, band position, and vapor pressure. The only obvious trend is that a strongly absorbing species such as carbon tetrachloride has the largest %Δ values. This is not surprising since these samples are the most difficult to prepare due to the small mixing ratio, either as a gravimetric or as a static sample.

Finally, neither NIST nor PNNL have corrected for sample emission in their corresponding spectral libraries. Sample emission is a known problem for the spectral region below ≈1100 cm^{-1} and in general gives rise to an apparent increase in the absorption cross-section.[35] A systematic study of the effect of sample emission as a function of sample temperatures has been discussed by Chu et al.[36] They found that the uncorrected methanol vapor spectrum at 25 °C (integrated between 900 cm^{-1} and 1150 cm^{-1}) was 0.4% greater than the corrected spectrum. A similar analysis for sulfur dioxide (1010 cm^{-1} to 1275 cm^{-1}) yielded an error of 0.9%. At higher temperature (50 °C) the errors increased to 1.0% and 1.8% for methanol and SO_2, respectively.

SUMMARY

Ultimately the databases will contain the high-resolution (0.1 cm^{-1}) quantitative pressure-broadened infrared spectra of several hundred gas-phase compounds. The spectral resolution is sufficient to bring out all sharp features, while also realizing that pressure broadening will dictate a line width ≥0.1 cm^{-1} in most cases. All data have been calibrated on the wavelength axis using secondary standards. We have demonstrated that both the flowing and static methods can yield accurate, reproducible, and linear absorption cross-sections that are applicable to laboratory and remote sensing spectroscopy. Provided that the data collection methods are carefully planned and executed, both the flowing and static methods have demonstrated excellent agreement for a host of different molecules.

The two databases, using entirely different sample quantitation methods, have further been compared against one another using species that range significantly in polarity, oscillator strength, and volatility. Several sources of artifacts and nonlinearity have been investigated, and these have either been redressed or accounted for in the data analysis. The two laboratories used different methods of sample generation to investigate possible systematic errors. Cross-comparison with 12 species showed an rms deviation of 1.66% for integrated band intensities, well within the 3.2% composite error estimate. Data continue to be collected for these libraries.

ACKNOWLEDGMENT

PNNL is operated for the U.S. Department of Energy by the Battelle Memorial Institute under contract DE-AC06-76RLO 1830.

1. R. J. Bell, *Introductory Fourier Transform Spectroscopy* (Academic Press, New York, 1972).
2. *Compendium of Methods for the Determination of Toxic Organic Compounds in Ambient Air*, EPA/625/R-96/010b (1999), 2nd ed.
3. U.S. Environmental Protection Agency (EPA) Method-320, *Measurement of Vapor Phase Organic and Inorganic Emissions by Extractive Fourier Transform Infrared Spectroscopy* (1999).
4. R. M. Measures, *Laser Remote Chemical Sensing*, Chemical Analysis, **94** (Wiley Interscience, New York, 1988).
5. L. R. Brown, M. R. Gunson, R. A. Toth, F. W. Irion, C. P. Rinsland, and A. Goldman, Appl. Opt. **35,** 2828 (1996).
6. N. Jacquinet-Husson, et al., J. Quant. Spectrosc. Radiat. Transfer **62,** 205 (1999).
7. N. Husson, B. Bonnet, N. A. Scott, and A. Chedin, J. Quant. Spectrosc. Radiat. Transfer **48,** 509 (1992).
8. L. S. Rothman, et al., J. Quant. Spectrosc. Radiat. Transfer **60,** 665 (1998).
9. Midac Corporation, *Standards: Gas Phase Infrared Spectral Standards.* A collection of approximately 150 vapor-phase infrared spectra supplied in digital format. Midac Corporation, Irvine, CA. Available over the World Wide Web at http://www.midac.com.
10. P. Hanst, *Infrared Spectra for Quantitative Analysis of Gases*, Infrared Analysis Inc. A collection of 296 vapor-phase infrared spectra supplied in digital format. Infrared Analysis Corporation, Anaheim, CA. Available on the World Wide Web at http://www.infrared-analysis.com.
11. *NIST/EPA Gas-Phase Infrared Database.* Available on the World Wide Web at http://www.nist.gov/srd/nist35.htm.
12. C. J. Pouchert, Ed., *The Aldrich Library of FT-IR Spectra Vapor Phase* (The Aldrich Chemical Comp. Inc., Milwaukee, WI, 1989), vol. 3, 1st ed.
13. P. M. Chu, F. R. Guenther, G. C. Rhoderick, and W. J. Lafferty, J. Res. Natl. Inst. Stand. Technol. **104,** 59 (1999).
14. J. R. Birch and F. J. J. Clarke, Spectrosc. Eur. **7,** 16 (1995).
15. R. C. M. Learner, A. P. Thorne, and J. W. Brault, Appl. Opt. **35,** 2947 (1996).
16. L. Mertz, Infr. Phys. **7,** 17 (1967).
17. D. B. Chase, Appl. Spectrosc. **36,** 240 (1982).
18. R. C. M. Learner, A. P. Thorne, I. Wynne-Jones, J. W. Brault, and M. C. Abrams, J. Opt. Soc. Am. A **12,** 2165 (1995).
19. J. W. Johns, Mikrochim. Acta **111,** 171 (1987).
20. D. B. Chase, Appl. Spectrosc. **38,** 491 (1984).
21. M. Birk, D. Hausamann, G. Wagner, and J. W. Johns, Appl. Opt. **35,** 2971 (1996).
22. J. Ballard, R. J. Knight, D. A. Newnham, J. Vander Auwera, M. Herman, G. Di Lonardo, G. Masciarelli, F. M. Nicolaisen, J. A. Beukes, L. K. Christensen, R. McPheat, G. Duxbury, R. Freckleton, and K. P. Shine, J. Quant. Spectrosc. Radiat. Transfer **66,** 109 (2000).
23. M. C. Abrams, G. C. Toon, and R. A. Schindler, Appl. Opt. **33,** 6307 (1994).
24. R. L. Richardson, Jr., H. Yang, and P. R. Griffiths, Appl. Spectrosc. **52,** 572 (1998).

25. A. Keens and A. Simon, US Patent #4,927,269, ''Correction of Non-linearities in Detectors in Fourier Transform Spectroscopy'', May 22 (1990).
26. J. E. Bertie, et al., Pure Appl. Chem. **70,** 2039 (1998).
27. T. J. Johnson, R. L. Sams, T. A. Blake, S. W. Sharpe, and P. M. Chu, Appl. Opt. **41,** 2831 (2002).
28. J. W. Johns, ''Thermal artifacts in mid- to far-IR FT spectroscopy'', in *Fourier Transform Spectroscopy: New Methods and Applications,* Vol. 4, 26OSA Technical Digest Series (Optical Society of America, Washington, D.C., 1995).
29. L. P. Giver, C. Chackerian, Jr., and M. N. Spencer, ''Thermal Contamination of BOMEM FTIR Line Shapes'', High Resolution Fourier Transform Spectroscopy 1992 Technical Digest (Optical Society of America, Washington, D.C., 1992), vol. 21.
30. R. A. Toth, J. Opt. Soc. Am. B **8,** 2236 (1991); R. A. Toth, J. Opt. Soc. Am. B **10,** 2006 (1993).
31. A. G. Maki and J. S. Wells, *Wavenumber Calibration Tables from Heterodyne Frequency Measurements,* NIST Special Publication 821, National Institute of Standards and Technology, Special Publication 821 (U.S. Government Printing Office, Washington, D.C. 1991). Available on the World Wide Web at http://physics.nist.gov/PhysRefData.
32. R. L. Richardson, Jr. and P. R. Griffiths, Appl. Spectrosc. **52,** 143 (1998).
33. S. W. Sharpe, R. L. Sams, T. J. Johnson, P. M. Chu, G. C. Rhoderick, and F. R. Guenther, ''Creation of 0.10 cm^{-1} Resolution, Quantitative, Infrared Spectral Libraries for Gas Samples'', in *Vibrational Spectroscopy-based Sensor Systems,* S. D. Christesen and A. J. Sedlacek III, Eds., Proc. SPIE-Int. Soc. Opt. Eng. **4577,** 12 (2002).
34. J. R. Taylor, *An Introduction to Error Analysis; the Study of Uncertainties in Physical Measurements* (University Science Books, California, 1997), 2nd ed., pp. 181–207.
35. J. Ballard, J. J. Remedios, and H. K. Roscoe, J. Quant. Spectrosc. Radiat. Transfer **48,** 733 (1992).
36. P. M. Chu, G. C. Rhoderick, and P. A. Johnson, ''Infrared Absorptive Temperature Dependence of Gas Phase Methanol and Sulfur Dioxide'', NISTIR 6773, (National Institute of Standards and Technology, Gaithersburg, MD, 2001).

APPENDIX

The NIST Quantitative Infrared Database can be obtained by registering on line at http://www.nist.gov/srd/nist79.htm. The database program is supplied on CD and requires Windows NT (version 4.00 or later), Windows 95, or Windows 98. An internet connection is required to download new files as they become available. Spectral data files are in JCAMP format and available in an assortment of apodizations and spectral resolutions. Spectral data is offered at a single temperature of 25 °C. All spectral files are accompanied by a short metadata file describing samples and their purity. Data distribution through the NIST Chemistry Web Book will become available at http://webbook.nist.gov/chemistry.

The PNNL Quantitative Infrared Database can be obtained by registering on line at http://nwir.pnl.gov. The database is supplied through internet download in both text (ASCII) and Thermo Electron Corporation's Grams (binary) format. The spectral data is supplied at $\Delta\nu$ = 0.112 cm^{-1} resolution using boxcar apodization. Spectral data is offered at 5, 25, and 50 °C, when chemical properties are amenable. All spectral files are accompanied by a metadata file (pdf format) describing sample conditions, instrumental conditions, and post-processing operations. In addition, a ''quick look'' file (pdf format) containing plots of the absorbance versus wavenumber and a vapor pressure versus temperature curve are included.

TABLE AI. Current data holdings for the NIST Quantitative Infrared Database (July 2004, http://webbook.nist.gov/chemistry).

1-Butanol	1,1-Dichloroethene	1,1,1-Trichloroethane	1,1,2-Trichloroethane
1,2-Dichloroethane	1,2-Dimethylbenzene	1,3 Butadiene	1,3-Dimethylbenzene
1,4-Dimethylbenzene	2-Propanol	Acetone	Acetonitrile
Acrylonitrile	Benzene	Bromomethane	Butane
Carbon Tetrachloride	Carbon Tetrafluoride	Chloroform	Dichlorodifluoromethane
Dichloromethane	Ethanol	Ethene	Ethyl Acrylate
Ethyl Acetate	Ethyl t-Butyl Ether	Ethylbenzene	Ethylene Oxide
Hexafluoroethane	Methanol	Methyl Ethyl Ketone	Methyl t-Butyl Ether
Pentafluoroethane	Propylene Oxide	Sulfur Dioxide	Sulfur Hexafluoride
Tetrachloroethene	Toluene	Trichloroethene	Vinyl Acetate

TABLE AII. Current data holdings for the PNNL Quantitative Infrared Database (July 2004).

1-Butene	1-Hexanoic acid	1-Nitropropane
1-Pentanol (n-amyl alcohol)	1-Propanethiol	1,1-Dichloroethane
1,1-Dimethylhydrazine	1,1,1-Chlorodifluoroethane	1,1,1-Trichloroethane
1,1,1-Trifluoroacetone	1,1,1,2-Tetrachloroethane	1,1,2-Trichloroethane
1,1,2,2-Tetrachloroethane	1,2-Dibomotetrafluoroethane	1,2-Dibromoethan
1,2-Dichloro-1,1,2-trifluoroethane	1,2-Dichloroethane	1,2-Dichloropropane
1,2-Diclorobenzene	1,2-Epoxybutane	1,3-Butadiene
1,3-Dichlorobenzene	1,3-Dichloropropane	1,3,5-Trimethylbenzene
1,4-Dichlorobenzene	2-Butane	2-Butoxyethanol
2-Chloroethanol	2-Chloroethyl ether	2-Chloropropane
2-Chlorotoluene	2-Chloro-1,1,1,2-tetrafluoroethane	2-Ethoxyethyl acetate
2-Ethyl-1-hexanol	2-Ethyltoluene	2-Fluoroethanol
2-Iodopropane	2-Mercaptoethanol	2-Methyl-1-butene
2-Methyl-1-propanol	2-Methyl-1,3-butadiene	2-Methyl-2-butene
2-Methyl-2-pentene	2-Methylpentane	2-Nitropropane
2-Pentanol	2-Propanethiol	2,2-Dichloro-1,1,1-trifluoroethane
2,2-Dimethyl butane	Texanol	3-Chlorotoluene
3-Ethyltoluene	3-Methyl-1-butene	3-Methylpentane
4-Chlorotoluene	4-Ethyltoluene	4-Methyl-1-pentene
Acetic acid	Acetic anhydride	Acetone
Acetone cyanohydrin	Acetyl chloride	Acetylaldehyde
Acetylene	Acrolein	Acrylol chloride
Allene	Allyl alcohol	Allyl bromide

TABLE AII. Continued.

Allyl chloride	Allyl iodide	Allyl isothiocyanate
Allylamine	alpha-Pinene (1S) (−)	Ammonia anhydrous
Arsine	Benzaldehyde	Benzene
Benzenethiol	Benzonitrile	Benzyl bromide
Benzyl chloride	beta-Pinene (1S) (−)	bis(2-Chloroethyl) ether
Boron tribromide	Boron trichloride	Boron trifluoride
Bromobenzene	Bromochlorodifluoromethane	Bromochloromethane
Bromotrifluoromethane	Butyl acetate	Butyraldehyde
Butyric acid	Cadaverine	Carbon dioxide
Carbon disulfide	Carbon monoxide	Carbon tetrachloride
Carbonyl fluoride	Carbonyl sulfide	Chloroacetone
Chloroacetonitrile	Chlorobenzene	Chloroethane
Chloromethyl ethyl ether	Chloromethyl methyl ether	Chloropicrin
Chlorosulfonyl isocyanate	Chlorotrifluoroethylene	Chlorotrifluoromethane
cis-1,3-Dichloropropene	cis-4-Methyl-2-pentene	Cumene
Cyanogen	Cyanogen chloride	Cyclohexane
Cyclohexanol	Cyclohexane	Cyclopentene
Cyclopropane	d-Limonene	Diborane
Dibromomethane	Dichlorofluoromethane	Dichloromethane
Dichlorosilane	Diethyl ether	Diethyl sulfate
Diethylamine	Diethylketone	Difluorodibromomethane
Diisopropylamine	Diketene	Dimethoxymethane
Dimethyl disulfide	Dimethyl ether	Dimethyl sulfide
Dimethyl sulfoxide	Dimethylamine	Ethane
Ethyl acetate	Ethyl alcohol	Ethyl benzene
Ethyl bromide	Ethyl cyanide	Ethyl formate
Ethyl methyl ether	Ethyl nitrite	Ethylamine
Ethylene	Ethylene glycol	Ethylene oxide
Ethylene sulfide	Ethylenediamine	Ethylvinyl ether
Fluorobenzene	Formaldehyde	1,1,2-Trichlorortrifluoroethane
1,2-Dichlorortetrafluoroethane	Dichlorodifluoromethane	Pentafluoroethane
1,1,1,2-Tetrafluoroethane	Octafluoropropane	Octafluorocyclobutane
Furan	Germane	Hexachlorocyclopentadiene
Hexafluoroacetone	Hexafluoroethane	1,1,2,2-Tetrafluoroethane
Hydrazine	Hydrogen bromide	Hydrogen chloride
Hydrogen cyanide	Hydrogen fluoride	Hydrogen iodide
Hydrogen sulfide	Iron pentacarbonyl	Isoamyl alcohol
Isobutane	Isobutene	Isooctane
Isopentane	Isopropyl acetate	Isopropyl alcohol
Isopropylamine	m-Cresol	m-Xylene
Methacryloyl chloride	Methane	Methanesulfonyl chloride
Methyl acetate	Methyl acrylate	Methyl acrylonitrile
Methyl alcohol	Methyl bromide	Methyl butyl ether
Methyl chloride	Methyl fluoride	Methyl formate
Methyl iodide	Methyl isobutyl ketone	Methyl isocyanate
Methyl isothiocyanate	Methyl mercaptan	Methyl methacrylate
Methyl nitrite	Methylamine	Methylchloroformate
Methyldichlorodisilanes	Methylethyl ketone	Methyltrichlorosilane
Methylvinyl ketone	Monomethyl hydrazine	n-Butane
n-Butyl alcohol	n-Butyl nitrite	n-Butylamine
n-Heptene	n-Hexane	Nickel carbonyl
Nicotine	Nitric acid, anhydrous	Nitric oxide
Nitrobenzene	Nitroethane	Nitrogen dioxide
Nitrogen trifluoride	Nitromethane	Nitrosyl chloride
Nitrous oxide	N,N′-Dimethyl formamide	N,N-Diethylaniline
o-Xylene	Octane	p-Xylene
Paraldehyde	Pentane	Perfluorobutane
Phosgene	Phosphine	Phosphorous oxychloride
Propane	Propylene	Propylenimine
Propyne	Pyridine	Quinoline
Silane	Silicon tetrafluoride	Sulfur dioxide
Sulfur hexafluoride	Sulfuryl chloride	Sulfuryl fluoride
Tetrafluoromethane	Tetrahydrofuran	Thiophosgene
Thiophosphoryl chloride	Titanium tetrachloride	Toluene
trans-1,2-Dichloroethene	trans-1,3-Dichloropropene	trans-Crotonaldehyde
Tribromomethane	Trichloroacetyl chloride	Trichloroethylene
Triethylamine	Trifluoroacetic acid	Trifluoroacetic anhydride
Trifluoroacetyl chloride	Trifluoromethane	Trifluoromethylsulfur pentafluoride
Trifluoronitrosomethane	Trimethylamine	Tungsten hexafluoride
Vinyl chloride	Water	Water-d1